Supplementary Materials for

Control of ribosomal subunit rotation by elongation factor G

Arto Pulk and Jamie H. D. Cate*

*Correspondence to: J. Cate (jcate@lbl.gov).

Supplementary Methods

Ribosome purification and crystallization.

Part of the ribosomal protein L9 gene encoding amino acids 56 to the C-terminus was deleted from *Escherichia coli* strain MRE600 by replacement with a kanamycin resistance gene using phage λ Red recombination as described (*58*). The L9 N-terminal globular domain still binds the 50S subunit in this strain (*59*), while making it possible to form crystals with EF-G (*60*). Ribosomes lacking protein S1 were purified from this strain following sucrose gradient centrifugation, as previously described (*61*). N-terminally His-tagged EF-G from *E. coli* was overexpressed in *E. coli* using vector pET-15 (Novagen), purified on a Ni-NTA affinity column, after which the His-tag was removed using TEV protease. The untagged protein was further purified by gel filtration and ion-exchange chromatography.

70S ribosomes were crystallized at 18 °C using microbatch 96-well plates and buffers containing 3.5% 2-methyl-2,4-pentanediol (MPD), 4.0–4.5% PEG 8000, 4.0 mM MgOAc, 30 mM NH_4Cl, 120 mM KSCN, 4 mM putrescine, 1 mM spermidine, 10 mM Tris, 40 mM MES, pH 6.5–7.0, and 0.25 mM EDTA. Ribosome complexes were formed by incubating 8 μM mRNA of sequence 5′- GGCAAGGAGGUAAAAUUCUACAAA-3′ (Thermo Scientific) with 2 μM ribosomes at 37 °C for 15 min. Ribosome recycling factor (RRF) was then added at a concentration of 15 μM, and the samples were incubated for an additional 15 min at 37 °C. Before adding EF-G and the nonhydrolyzable GTP analog GMPPCP to the ribosome complexes, the 70S ribosome-RRF complex was treated with 500 μM of the antibiotic viomycin (USP) and incubated 10 min at 37 °C. The final ribosome complex was then formed at 37 °C for 10 min with EF-G preincubated with GMPPCP at concentrations of 15 μM EF-G and 1 mM GMPPCP (Sigma-Aldrich). The different crystal forms reported here were obtained using similar biochemical procedures, but were prepared from different preparations of ribosomes and reagents.

X-ray data collection and processing.

Ribosome crystals were stabilized with crystallization buffer containing 20 mM MgOAc, 100 mM KSCN, 4 mM putrescine, 1 mM spermidine, 7.0% MPD, 6.0% PEG 8000 and 28% PEG 400, pH 6.5, to allow cryo-cooling of the crystals to liquid nitrogen temperatures. Crystals were frozen with liquid nitrogen after 1 day of incubation at 4 °C. Diffraction data were

measured from crystals cooled to 100 K using 0.1–0.3° oscillations at the Advanced Light Source (beamlines 8.3.1 and 12.3.1), each of which is equipped with an ADSC Q315 area detector. Data were reduced using XDS (*62*), yielding the statistics shown in Table S1. The high-resolution cut-off was chosen using the recently defined correlation factor CC(1/2) that is a useful indicator of crystallographic information in each resolution shell (*54*).

Molecular replacement and structure refinement.

The four copies of the 70S ribosome in the crystallographic asymmetric unit were located using molecular replacement in PHENIX (*63*), with *E. coli* ribosomes from the recent atomic-resolution structure determination used as search models (*19*). Refinement was carried out in PHENIX with torsional non-crystallographic (NCS) restraints (*63*). Corrections to the resulting model were carried out manually in Coot (*64*). Difference electron density maps were generated from the PHENIX output directly and noncrystallographic symmetry (NCS) and cross-crystal averaged maps were generated using the Rave software suite (*65*). EF-G modeling was carried out iteratively in Coot and PHENIX using the previously-determined structure of *T. thermophilus* EF-G bound to the ribosome in a complex with GDP and fusidic acid (*32*).

No electron density was observed for RRF, indicating that RRF was released from the 70S ribosome in the presence of viomycin, and/or EF-G bound to the GTP analogue. It has been shown that EF-G releases RRF from 70S ribosomes but not from 50S ribosomal subunit complexes (*66*). The release of bound RRF by EF-G is stimulated by GTP analogues (*66*). Furthermore, the EF-G-dependent release of RRF occurs in the presence of viomycin (*66*). In the present crystals, crystal packing between adjacent ribosomes in the asymmetric unit precludes tRNA binding in the large subunit E site, due to the cross-ribosome positioning of ribosomal protein L1 in the E site. There are no crystal contacts to EF-G in any of the ribosome structures in these crystal forms.

In (F_{obs} –F_{calc}) difference electron density maps, viomycin was observed bound in the decoding site in 7 of 8 ribosomes. However, the viomycin electron density in crystal form II is much weaker than that in crystal form I in the final ($2F_{obs}$ – F_{calc}) electron density maps (Supplementary Figure 4C, 4D). Furthermore, the viomycin molecules in crystal form II refine to a much lower occupancy (i.e. stoichiometry) in the final models, and probably overestimate the extent of binding based on the level of electron density in the final ($2F_{obs}$ – F_{calc}) maps. The weaker binding of viomycin to ribosomes in crystal form II likely resulted from more extensive ultrafiltration of the ribosome complexes prior to crystallization in these experiments, or from viomycin decomposition in the stock solutions over time.

Together with the present structures, in which viomycin binds ribosomes in an intermediate state of rotation, viomycin binding to h44 can occur to all rotational states, as viomycin binding has been observed in unrotated (*67*) and fully rotated ribosomes (*68*). The fact that we observe partially-rotated and fully-rotated ribosomes both in the absence and presence of viomycin binding rules out that viomycin is responsible for the rotated states observed in 7 of 8 ribosomes. The observation of one unrotated ribosome in the absence of viomycin is consistent with observations that viomycin stabilizes the rotated state (*23, 69*). In the partially-rotated

ribosomes (Crystal form I), the β-lysine moiety of viomycin adopts a conformation observed previously (*67, 68*) (fig S4A) or in a bent conformation not seen before (fig S4B).

Superpositions.

Comparisons to atomic-resolution structures of the ribosome were carried out by the 'pair_fit' command in PyMOL (*70*) or by least-squares superposition in the program O (*71*). Disordered or moving regions of 23S rRNA were not used in the superpositions, for example the L1 stalk, the L7/L12 stalk, and 23S rRNA helices H38 and H69. Superpositions of ribosomal RNA were performed using nucleotide ribose C1′ positions or phosphorus atoms. The angles of rotation of the 30S subunit domains were calculated essentially as described previously (*19*). Angles given for the rotation of the head domain were calculated from 30S subunit structures superimposed by means of their platform domains. A rotation of 0° is defined as centering the head domain over the 30S P site, as seen in the structure of the unrotated ribosome with tRNA positioned in the P site of both the 30S and 50S ribosomal subunits (*19*).

Figure preparation.

All structure figures were made using the program PyMOL (*70*).

Table S1. Conformations of the 30S subunit in different ribosomal states

Ribosome (crystal form)	30S body/platform rotation[1]	30S head domain rotation[2]
Intermediate rotation #1 (I)	4°	9°
Intermediate rotation #2 (I)	4°	6°
Intermediate rotation #3 (I)	3°	7°
Full rotation (I)	7°	11°
Intermediate rotation #1 (II)	4°	10°
Intermediate rotation #2 (II)	4°	9°
Unrotated (II)	0°	10°
Full rotation (II)	8°	10°

[1]Rotation of the 30S subunit body/platform domains calculated with respect to the 50S subunit as a frame of reference.
[2]Rotation or swiveling of the 30S subunit head domain calculated with respect to the 30S platform domain.

Supplementary Figures

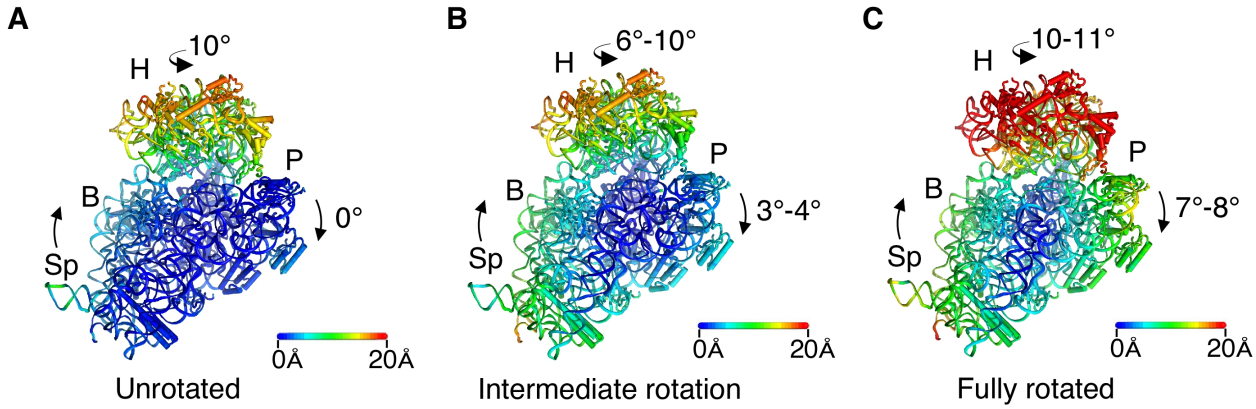

Figure S1. Overall conformation of 70S ribosomes in EF-G/GMPPCP complexes. (**A**) Ribosome in an unrotated state of subunit rotation. The rotation is shown relative to the unrotated state with P-site tRNA bound (PDB 4GD2) (*19*), using the 50S ribosomal subunit as a frame of reference. Difference vectors are between corresponding phosphorous or Cα atoms in the two 30S subunits. (**B**) Ribosome in an intermediate state of subunit rotation with a large swiveling of the 30S subunit head domain. (**C**) 70S ribosome in a fully rotated state. In panels A – C, the ribbon and difference vectors are color-coded by the distance between corresponding atoms in the ribosome and the reference structure, the unrotated state. In panels B and C, the ranges of rotation angles seen for the ribosomes in the two crystal forms are indicated.

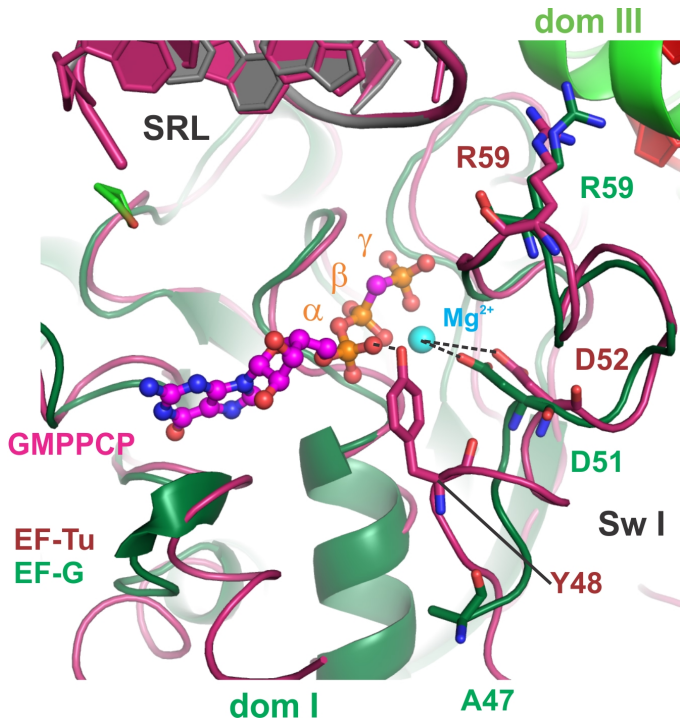

Figure S2. Differences between the geometry of switch I in EF-G and EF-Tu. The conformation of swI region 45-49 of EF-Tu (red) (*6*) (PDB entries 2XQD, 2XQE) has an extended loop where Tyr48 interacts with the α-phosphate of GTP. In the EF-G structure (dark green) region 47-49 (complementary to the EF-Tu 45-49 region) has a shorter loop and does not interact with the α-phosphate of GTP. This region has high variability between different GTPase factors and Y48 in EF-Tu is replaced with A49 in EF-G (*1*).

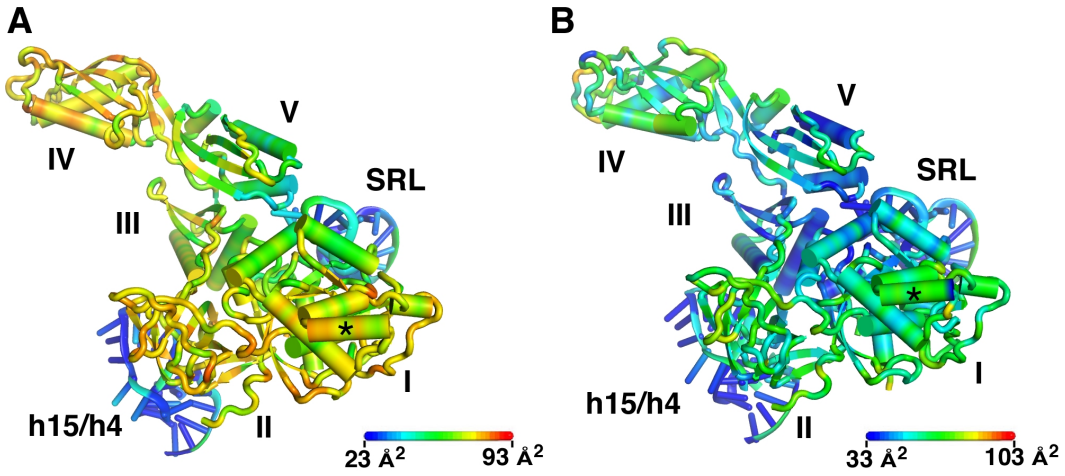

Figure S3. Comparison of EF-G/GMPPCP conformations in different ribosomal states. (**A**) Ribbon diagram of EF-G/GMPPCP bound to the unrotated state of the ribosome, colored by residue-specific atomic displacement parameters (B-factors), which reflect the extent of disorder. Scale bar indicates the range of colors for B-factors. (**B**) Ribbon diagram of EF-G/GMPPCP bound to the fully-rotated state of the ribosome, colored by residue-specific atomic displacement parameters, which reflect the extent of disorder. Scale bar indicates the range of colors for B-factors. B-factor ranges in both panels were chosen to normalize the relative order of the ribosomes.

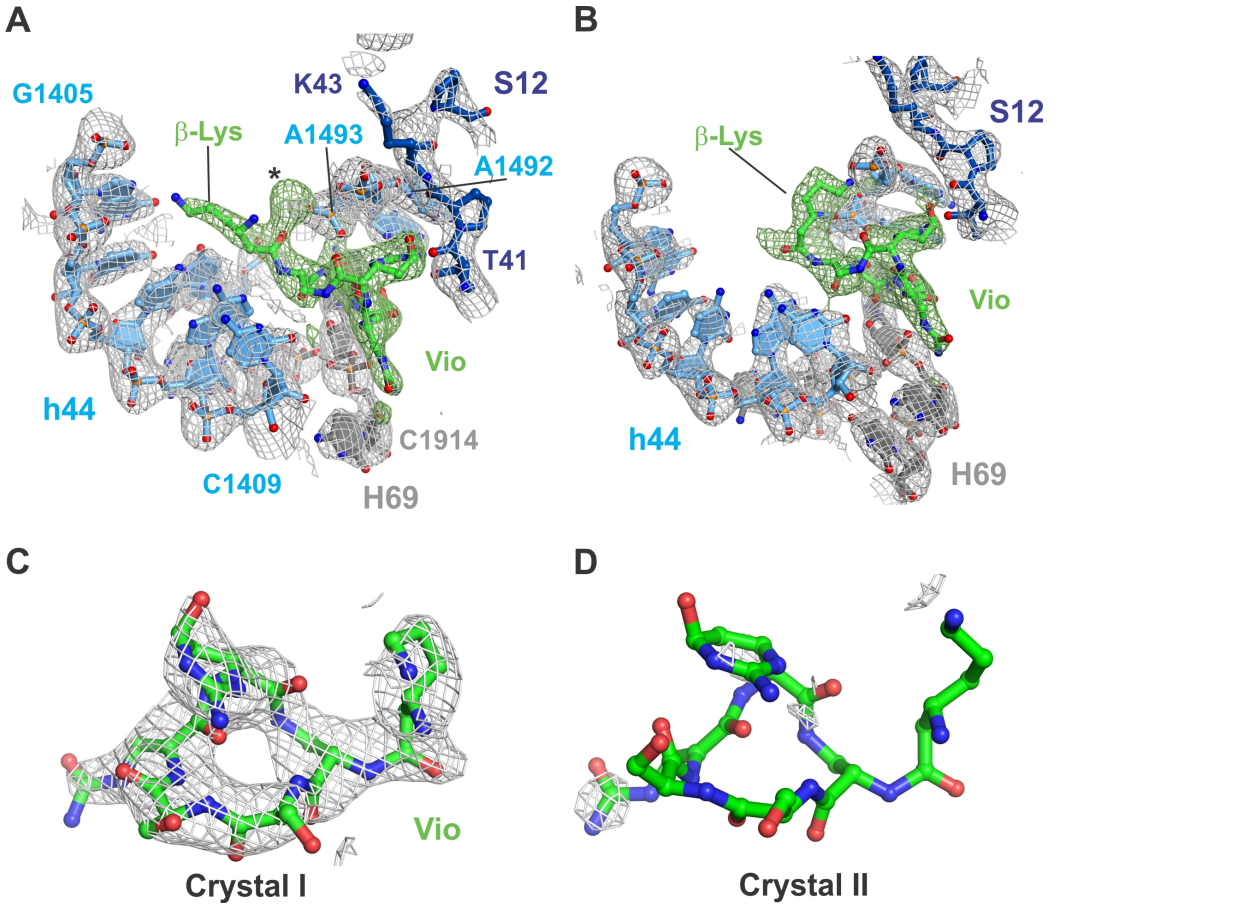

Figure S4. Viomycin binding to ribosomes in intermediate rotation states, in the presence of EF-G complexed with the GTP-analog GMPPCP. (**A**) Viomycin binding site in 16S rRNA helix h44. (F_{obs}-F_{calc}) difference electron density is shown for viomycin (green) or ($2F_{obs}$-$2F_{calc}$) difference electron density for 16S rRNA helix h44 (light blue), 23S rRNA helix H69 (grey), and ribosomal protein S12 (dark blue). The (F_{obs}-F_{calc}) difference electron density (green) is shown at a contour of 3 standard deviations from the mean and the ($2F_{obs}$-F_{calc}) difference electron density (grey) is shown at a contour of 1.4 standard deviations from the mean**.** The viomycin β-lysine moiety is extended, as seen in previous ribosome bound structures (*67, 68*). The asterisk indicates extra electron density that may correspond to an alternative conformation of the β-lysine, as shown in panel B. (**B**) Viomycin β-lysine moiety is in a bent conformation not seen before. All the markings and color-coding are the same as in panel A. (**C**) The ($2F_{obs} - F_{calc}$) electron density map for viomycin bound to an intermediate-rotated ribosome in crystal form I. ($2F_{obs} - F_{calc}$) electron density is shown at a contour of 1.1 standard deviations from the mean. (D) The ($2F_{obs} - F_{calc}$) electron density map for viomycin bound to the related intermediate-rotated ribosome in crystal form II. The ($2F_{obs} - F_{calc}$) electron density is shown at a contour of 1.1 standard deviations from the mean.

Supplementary References

58. K. A. Datsenko, B. L. Wanner, "One-step inactivation of chromosomal genes in Escherichia coli K-12 using PCR products." *Proc Natl Acad Sci U S A* **97**, 6640 (Jun 6, 2000).

59. K. R. Lieberman, M. A. Firpo, A. J. Herr, T. Nguyenle *et al.*, "The 23 S rRNA environment of ribosomal protein L9 in the 50 S ribosomal subunit." *J Mol Biol* **297**, 1129 (Apr 14, 2000).

60. M. Selmer, Y. G. Gao, A. Weixlbaumer, V. Ramakrishnan, "Ribosome engineering to promote new crystal forms." *Acta Crystallogr D Biol Crystallogr* **68**, 578 (May, 2012).

61. B. S. Schuwirth, M. A. Borovinskaya, C. W. Hau, W. Zhang *et al.*, "Structures of the bacterial ribosome at 3.5 A resolution." *Science* **310**, 827 (Nov 4, 2005).

62. W. Kabsch, "Xds." *Acta Crystallogr D Biol Crystallogr* **66**, 125 (Feb, 2010).

63. P. D. Adams, P. V. Afonine, G. Bunkoczi, V. B. Chen *et al.*, "PHENIX: a comprehensive Python-based system for macromolecular structure solution." *Acta Crystallogr D Biol Crystallogr* **66**, 213 (Feb, 2010).

64. P. Emsley, B. Lohkamp, W. G. Scott, K. Cowtan, "Features and development of Coot." *Acta Crystallogr D Biol Crystallogr* **66**, 486 (Apr, 2010).

65. G. J. Kleywegt, R. J. Read, "Not your average density." *Structure* **5**, 1557 (Dec 15, 1997).

66. M. C. Kiel, V. S. Raj, H. Kaji, A. Kaji, "Release of ribosome-bound ribosome recycling factor by elongation factor G." *J Biol Chem* **278**, 48041 (Nov 28, 2003).

67. R. E. Stanley, G. Blaha, R. L. Grodzicki, M. D. Strickler, T. A. Steitz, "The structures of the anti-tuberculosis antibiotics viomycin and capreomycin bound to the 70S ribosome." *Nat Struct Mol Biol* **17**, 289 (Mar, 2010).

68. J. Zhou, L. Lancaster, S. Trakhanov, H. F. Noller, "Crystal structure of release factor RF3 trapped in the GTP state on a rotated conformation of the ribosome." *RNA* **18**, 230 (Feb, 2012).

69. D. N. Ermolenko, P. C. Spiegel, Z. K. Majumdar, R. P. Hickerson *et al.*, "The antibiotic viomycin traps the ribosome in an intermediate state of translocation." *Nat Struct Mol Biol* **14**, 493 (Jun, 2007).

70. W. L. Delano, in *Delano Scientific, San Carlos, CA, USA.* (2002).

71. T. A. Jones, J. Y. Zou, S. W. Cowan, M. Kjeldgaard, "Improved methods for building protein models in electron density maps and the location of errors in these models." *Acta Crystallogr A* **47 (Pt 2)**, 110 (Mar 1, 1991).